



Cobalt–iron red–ox behavior in nanostructured $\text{La}_{0.4}\text{Sr}_{0.6}\text{Co}_{0.8}\text{Fe}_{0.2}\text{O}_{3-\delta}$ cathodes

Analía L. Soldati*, Laura Baqué¹, Federico Napolitano, Adriana Serquis

CONICET—CNEA Departamento de Caracterización de Materiales, Centro Atómico Bariloche, Av. Bustillo 9500, S.C. de Bariloche R8402AGP, Río Negro, Argentina

ARTICLE INFO

Article history:

Received 14 August 2012

Received in revised form

17 October 2012

Accepted 18 October 2012

Available online 26 October 2012

Keywords:

LSCF

Cathodes

Fuel cell

Perovskite

B-site

ABSTRACT

Nano-sized $\text{La}_{0.4}\text{Sr}_{0.6}\text{Co}_{0.8}\text{Fe}_{0.2}\text{O}_{3-\delta}$ (LSCF) perovskite samples (prepared by a conventional acetate route and a novel acetate synthesis with HMTA additives), were tested simulating a red–ox cycle. The crystallography was studied by X-ray Powder Diffraction (XPD) and the changes in the oxidation state of the perovskite B-site were evaluated by synchrotron X-ray Absorption Near Edge Spectroscopy (XANES). After a reducing treatment, LSCF particles show the appearance of a new phase that coexists with the original one. The structural change is accompanied by a Co and Fe formal oxidation states decrease, although Fe remains always closer to 4+ and Co closer to 3+. The treatment produces a B-site valence average reduction from 3.52+ to 3.26+ and the formation of oxygen vacancies. A re-oxidation treatment under O_2 rich atmosphere at 800 °C for 10 h shows that the change is reversible and independent of the two chemical methods used to synthesize the LSCF nano-particles.

© 2012 Elsevier Inc. All rights reserved.

1. Introduction

Much effort has recently been done investigating perovskite materials such as $\text{La}_{1-x}\text{Sr}_x\text{Co}_{1-y}\text{Fe}_y\text{O}_{3-\delta}$ (LSCF) as cathodes for solid oxide fuel cells (SOFC) [1–10]. These ceramics, appropriated for intermediate temperature (IT)–SOFC design, are especially interesting due to its ability to conduct both oxygen ions and electrons, thus enlarging the performance of the cell.

It is well known that different synthesis procedures, modification of the micro- and nanostructure, mechanical stress, substitution and/or addition of small quantities of dopants change the electronic structure of the cathode and may improve or, in the worst case, deteriorate the cell transport properties. We previously reported that a significant area specific resistance (ASR) reduction, with its consequent performance enhancement, could be achieved by reducing the grain size from the micrometric to the nanometric scale in $\text{La}_{0.4}\text{Sr}_{0.6}\text{Co}_{0.8}\text{Fe}_{0.2}\text{O}_{3-\delta}$ cathodes [5,6].

An important premise before the application of this material in real devices is to guarantee the long term phase stability and electrochemical performance at different conditions. Transitions to

phases showing oxygen vacancy ordering were observed in the $(\text{La,Sr})(\text{Co,Fe})\text{O}_{3-\delta}$ family after exposure to reductive thermal treatments [11–13]. For example, a transition to brownmillerite phase under low oxygen partial pressures was reported for sub-micrometric strontium-rich $\text{La}_{1-x}\text{Sr}_x\text{Co}_{0.8}\text{Fe}_{0.2}\text{O}_{3-\delta}$ compounds (i.e. $x \geq 0.7$) [12] leading to a deterioration of the cathode transport and mechanical properties. Nevertheless, no transition was observed in sub-micrometric $\text{La}_{0.4}\text{Sr}_{0.6}\text{Co}_{0.8}\text{Fe}_{0.2}\text{O}_{3-\delta}$ powders by X-Ray diffraction (XRD) in the 20–900 °C and $-5 \leq \log p\text{O}_2 \leq 0$ ranges. On the contrary, some unexpected lattice distortions were reported in the nanostructured $\text{La}_{0.4}\text{Sr}_{0.6}\text{Co}_{0.8}\text{Fe}_{0.2}\text{O}_{3-\delta}$ powders when they are exposed to reductive atmospheres (Ar) in the 150–600 °C range in comparison with those tested in an oxidative medium [14].

In this work, we aim to determine whether or not the distortions observed in nanocrystalline LSCF oxides imply the formation of new phases and/or chemical changes in the oxidation state of the transition metals (Co and Fe) occupying the B-site of the perovskite. For that, nanostructured $\text{La}_{0.4}\text{Sr}_{0.6}\text{Co}_{0.8}\text{Fe}_{0.2}\text{O}_{3-\delta}$ samples were analyzed *ex-situ* after different thermal treatments using reductive and oxidative atmospheres by X-ray Absorption Near Edge Spectroscopy (XANES) and X-ray Powder Diffraction (XPD).

2. Materials and methods

2.1. Sample preparation

Nanostructured powders of composition $\text{La}_{0.4}\text{Sr}_{0.6}\text{Co}_{0.8}\text{Fe}_{0.2}\text{O}_{3-\delta}$ (LSCF) were synthesized by a conventional acetate route and by the

* Correspondence to: Materials Characterization Department, Centro Atómico Bariloche, Av. Bustillo 9500, 8400 San Carlos de Bariloche, Río Negro, Argentina. Fax: +54 2944 445 100x5283.

E-mail addresses: asoldati@cab.cnea.gov.ar (A.L. Soldati), baque.laura@gmail.com (L. Baqué), napolitf@ib.cab.cnea.gov.ar (F. Napolitano), aserquis@cab.cnea.gov.ar (A. Serquis).

¹ Present address: Department of Energy Conversion and Storage, Risø Campus, Frederiksborgvej 399, DK-4000 Roskilde, Denmark.

Table 1
Synthesis methods and thermal treatments applied to the nano-sized $\text{La}_{0.4}\text{Sr}_{0.6}\text{Co}_{0.8}\text{Fe}_{0.2}\text{O}_{3-\delta}$ (LSCF) oxides used in this work.

Sample	Synthesis	Reduction	Oxidation
Acetates			
LSCF_A_ap	900 °C, 6 h		
LSCF_A_red	900 °C, 6 h	500 °C, Ar, 24 h	
LSCF_A_ox	900 °C, 6 h	500 °C, Ar, 24 h	800 °C, O ₂ , 10 h
HMTA			
LSCF_H_ap	900 °C, 6 h		
LSCF_H_red	900 °C, 6 h	500 °C, Ar, 24 h	
LSCF_H_ox	900 °C, 6 h	500 °C, Ar, 24 h	800 °C, O ₂ , 10 h

novel HTMA route [5]. In the following, all samples which were synthesized by the acetate or the HMTA method will be referred as *LSCF_A* and *LSCF_H*, respectively (Table 1). Two batches of each powder were sintered at 900 °C in air for 6 h. One batch of each synthesis was reserved and called “as prepared or ap” material. The rest was reduced in an Ar atmosphere at 500 °C for 24 h using 5 °C/min heating and cooling rates, named “red”. Subsequently, part of the reduced powders was oxidized in an O₂ rich atmosphere at 800 °C for 10 h using a 5 °C/min heating rate and a 1 °C/min cooling rate (called “ox”).

2.2. X-ray Powder Diffraction (XPD)

XPD measurements were performed using a Phillips PW 3710 diffractometer with $\text{CuK}\alpha$ radiation and a graphite monochromator. Diffractograms were collected over the $10^\circ < 2\theta < 90^\circ$ range with 0.02° step and 1 s/step counting time. Selected diffractograms were collected with higher counting time (12 s/step) in order to perform the Rietveld refinement using the FullProf Suite software [15].

2.3. X-ray Absorption Near Edge Spectroscopy (XANES)

LSCF powder samples were diluted with BN in ratio approximately 1:5 to get an absorption integral of 1 at the Co and Fe edge. The mixtures were pressed to pellets for the X-ray absorption measurements in transmission mode. Co and Fe references materials with different oxidation states were prepared and measured in the same way. The measurements were done in the beam line X04 of the Brazilian Synchrotron Light Laboratory, LNLS, Campinas, Brazil. Co *K*-edge and Fe *K*-edge XANES spectra were scanned three times in one point for the signal-to-noise ratio optimization and for the error bars evaluation. Three to six different points in the same pellet were measured and averaged to account for possible heterogeneities.

A Si (111) crystal was used as monochromator. The crystal was scanned from 200 eV below to 800 eV above the metal's *K* absorption edges. The measurements were done in transmission mode at room temperature. Energy steps of 0.5 and 2 eV were used for the XANES and the extended (EXAFS) region, respectively. A metallic foil was used in each case as a reference to calibrate for energy shifts. The foils were placed behind the sample along the direction of the X-ray beam. Following this procedure, the energy reproducibility between measurements resulted better than 0.1 eV (0.001% at the *K*-edge of the metal foils). Reference materials were measured in the same way as the samples for comparison of the valence state. Co (Co⁰), CoO (Co²⁺), Co₃O₄ (mixture 1:2 of Co²⁺ and Co³⁺), LaCoO₃ (Co³⁺) and BaCoO₃ (Co⁴⁺) were used as references for the element cobalt. In addition, selected compounds as Fe (Fe⁰), FeO (Fe²⁺), Fe₃O₄ (mixture 1:2 Fe²⁺ and Fe³⁺), and Fe₂O₃ (Fe³⁺) were used as reference for the different oxidation states of iron.

The composition of each reference was tested previously using X-Ray Diffraction.

The programs Athena[®] and Winxas[®] were used for calculation. Energy calibration was applied setting the first maximum of the first derivative of the Co⁰ reference foil equal to 7709.0 eV and of the Fe⁰ foil equal to 7112.0 eV. After background subtraction and normalization the edge position was taken as the position of the first intense maximum of the first derivative curve. The pre-edge feature of each spectrum was fitted using a spline function for the baseline subtraction and the convolution of Gaussian components with a FWHM between 1 and 3 eV.

2.4. Thermogravimetric balance analysis (TG)

Oxygen stoichiometry of the samples was independently determined by thermogravimetric measurements performed in a symmetrical thermobalance based on a Cahn 1000 electro balance [32] coupled to an electrochemical system for the measurement and control of *p*O₂ [33] with a similar method to that described in reference [12]. The same procedure was applied to both “as prepared” samples (*LSCF_H_ap* and *LSCF_A_ap*). Samples usually contain a non-negligible amount of adsorbed humidity, which may induce to errors in the calculated amount of oxygen, particularly in the as-prepared samples. Accordingly, the oxygen stoichiometry of the “as prepared” samples was determined at ≤ 250 °C, where the mass weight was stable after losing the adsorbed humidity and before starting to loss oxygen. A small quantity (i.e. 100–500 mg) of sample was heated in Ar up to 500 °C and cooling down again to room temperature after the equilibrium was reached (i.e. no mass change higher than 25 μg was recorded over a period of at least 8 h). The oxygen stoichiometry determined after this first cooling down is assumed to be the corresponding to the reduced samples (*LSCF_H_red* and *LSCF_A_red*). Afterwards, the sample was heated in pure oxygen up to 800 °C and cooling down again to room temperature after the equilibrium was reached. This latter value was considered to be equal to that of the re-oxidized samples (*LSCF_H_ox* and *LSCF_A_ox*). Finally, the sample was reduced in a 90% Ar/10% H₂ mixture at 1100 °C and cooled down to room temperature [12]. Oxygen non-stoichiometry (δ) was estimated assuming La₂O₃, SrO, Co and Fe as the final products, according to the following formula:

$$\delta_i = 1.8 - \left[\frac{M(m_i - m_f)}{16m_f} \right]$$

where δ_i is the oxygen non-stoichiometry in the condition *i*, m_i is the mass measured in the condition *i*, and m_f is the mass after the final reduction in 90% Ar/10% H₂ mixture.

3. Results and discussion

3.1. XPD results

Fig. 1A displays XPD data corresponding to HMTA samples before (*LSCF_H_ap*) and after (*LSCF_H_red*) a reductive thermal treatment in Ar for 24 h. The *LSCF_H_ap* sample can be indexed by the $R\bar{3}c$ spatial group (PDF Card 00-048-0124) with cell parameters $a=b=5.432$ Å and $c=13.294$ Å. A splitting of all peaks along with a decrease in intensity can be observed for the reduced sample (*LSCF_H_red*). This feature is particularly noticeable in the peak at $2\theta=47.5^\circ$, since the reflection (024) is the only one in $R\bar{3}c$ which contributes to this peak. In addition, a new low-intensity peak can be distinguished at $2\theta=11.5^\circ$ for the reduced sample. A similar trend was observed for the samples prepared by acetate

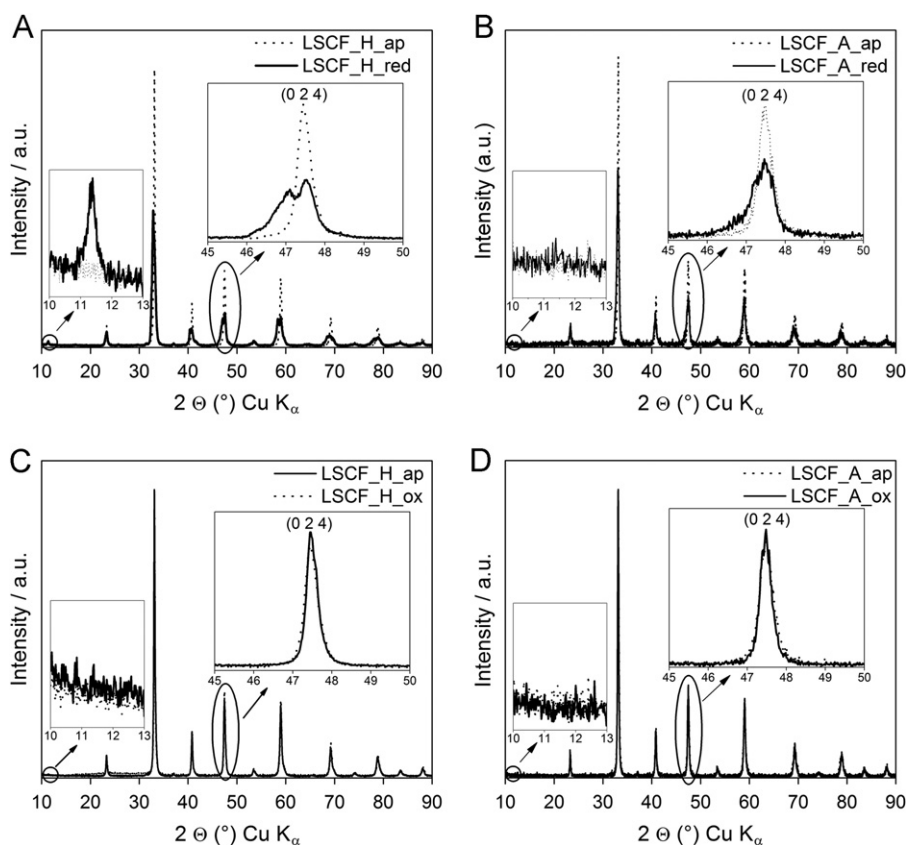


Fig. 1. X-ray diffractograms comparing the results of applying reduction (A and B) and re-oxidation treatments (C and D). The left column shows samples synthesized by the novel HMTA route (A and C). The right column (B and D) shows samples synthesized by an acetate route.

method (see Fig. 1B), although not so pronounced as in the HMTA samples.

The characteristics of the diffractograms corresponding to the reduced samples are similar to that observed for phases which present oxygen vacancy ordering such as $\text{A}_8\text{B}_8\text{O}_{23}$ and $\text{A}_2\text{B}_2\text{O}_5$ [11]. Accordingly, several attempts were made in order to refine the diffractograms by the Rietveld method, taking into account these phases alone as well as different combinations of them. The best results were obtained with a mixture of the perovskite phase ($\text{La}_{0.4}\text{Sr}_{0.6}\text{Co}_{0.8}\text{Fe}_{0.2}\text{O}_{3-\delta}$, $R\bar{3}c$ spatial group and cell parameters $a=b=5.453$ Å and $c=13.226$ Å) and the brownmillerite ($\text{La}_{0.8}\text{Sr}_{1.2}\text{Co}_{1.6}\text{Fe}_{0.4}\text{O}_5$) phase [11], this latter with lcm spatial group and cell parameters $a=5.537$ Å, $b=15.743$ Å and $c=5.478$ Å. The appreciable differences between the observed and the calculated intensity of some reflections imply that, although some oxygen vacancy ordering would exist, the crystallographic model should still be improved. Consequently, the analysis of neutron diffraction and high temperature synchrotron XPD data is in progress.

Fig. 1C and D shows X-ray diffractograms from re-oxidized samples (i.e. after applying a thermal treatment in pure oxygen at 800 °C for 10 h to the reduced samples). It can be seen that diffractograms from re-oxidized samples (LSCF_Hox and LSCF_Aox) are similar to those of the as-prepared samples (LSCF_Hap and LSCF_Aap), independently of the preparation method. Analogous results were obtained by applying the same thermal treatment to the reduced samples but using air instead of oxygen. All the above indicates that the phase transformation observed in Fig. 1A and B can be reverted by applying a suitable oxidizing thermal treatment.

Interestingly, this red–ox reaction, with appearance of a phase at the reduced state (with some degree of oxygen vacancies order) that coexists with the rhombohedral one, seems to occur

only in nano-sized LSCF. Powders of the same composition [12] or of the same family [4,7,10], but synthesized at higher temperatures (i.e. with micrometric grain size), did not show appreciable differences between the reduced and the as-prepared diffractograms (all reported as the rhombohedral $R\bar{3}c$ spatial group).

3.2. XANES results

For the XANES analyses three to six spectra were merged for each studied sample, increasing the confidence of the data. In this way, a comparison of the standard deviation was used to check for possible sample heterogeneities. This analysis was performed evaluating intensity and position differences at three characteristic spectral features of the normalized spectra: the white line (WL, maximal absorption peak of the XANES spectrum), the edge (maximum of the first intense peak of the first derivative of the absorption spectrum) and the shoulder (SH, a shoulder present also in the first derivative spectra of some samples at the left side of the edge peak).

Regarding the cobalt measurements (Fig. 2A), three scans in the same spot of a given LSCF sample introduced a maximal standard deviation of 0.19 eV (0.002%) in the positions of the WL, the SH or the edge, and 1.4%, 0.6% and 3.5% in their normalized intensities. On the other side, three to six measurements in different spots of the same sample showed a maximal standard deviation of 0.24 eV (0.003%) in the positions and 0.9%, 2.1% and 5.3% in the intensities, respectively.

The same statistical treatment was also applied on the Fe K-edge spectra (Fig. 2B); 3–6 scans in different points of a given LSCF sample produced a maximal standard deviation of 0.17 eV (0.002%) in the position of the edge, the WL or the SH and 1.7%, 2.7% and 14.7% in their normalized intensities. The

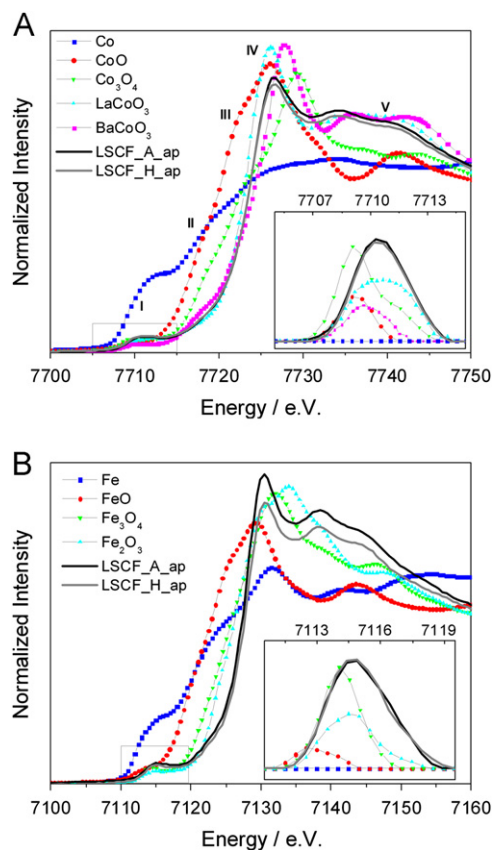


Fig. 2. Absorption coefficient for cobalt (A) and iron (B) in different reference materials compared to two LSCF *as-prepared* samples synthesized by two different methods (acetates and HMTA). The absorption intensity was normalized to 1 at the energy where no more EXAFS oscillations were observed. The pre-edge features after baseline subtraction are shown enlarged in the inset.

differences found are due to intrinsic characteristics of measurement or the sample itself. Thus, when comparing these spectral features in two different samples, higher deviations than those mentioned above are expected to have some other origin than a simple statistical error of the XAS measurement or heterogeneities inherent to the sample preparation.

3.2.1. Cobalt XANES

As shown in Fig. 2A, the absorption coefficient of Cobalt in two LSCF samples and different reference materials presents a main absorption jump between 7705 and 7725 eV. Different characteristic features (I–V) can be identified. The main peak (IV), also called the “white line” because of historical reasons, appears due to $1s \rightarrow 4p$ electrical dipole transition. Splitting of the $4p$ orbitals ($4p_{x,y,z}$) may produce some intermediate peaks on the edge region (labeled II and III) which are better observed, for example, in the Co₃O₄ and the CoO samples. The high energy part of the spectra (V) is more sensitive to structural parameters like the neighbor’s identity and their coordination with the absorbing atom. Thus, peaks appearing to the right side of the white line reflect local structure variations. On the low energy side, a low-intensity peak around 7709 eV (labeled I) can be clearly observed in all samples, except for metallic Co. This “pre-edge” peak (enlarged in the inset of Fig. 2A) is related to transition to the $3d$ bands of transition metals [16]. It reflects electric quadrupolar $1s \rightarrow 3d$ transitions and, in some cases, also electric dipolar transitions in which the $3d$ level presents more p character due to p – d mixing [16] and hybridization with oxygen orbitals [17,18].

Both LSCF *as prepared* materials show very similar absorption coefficients, displaying their pre-edge peaks (I) and WL (IV) with almost the same intensity and FWHM. Even the first derivative of the spectra coincides in positions and intensities (not shown) and the high energy part of the spectra (V) follows the same form, presenting only slight intensity differences. Thus, this data supports that Co is in the same oxidation state and environment in

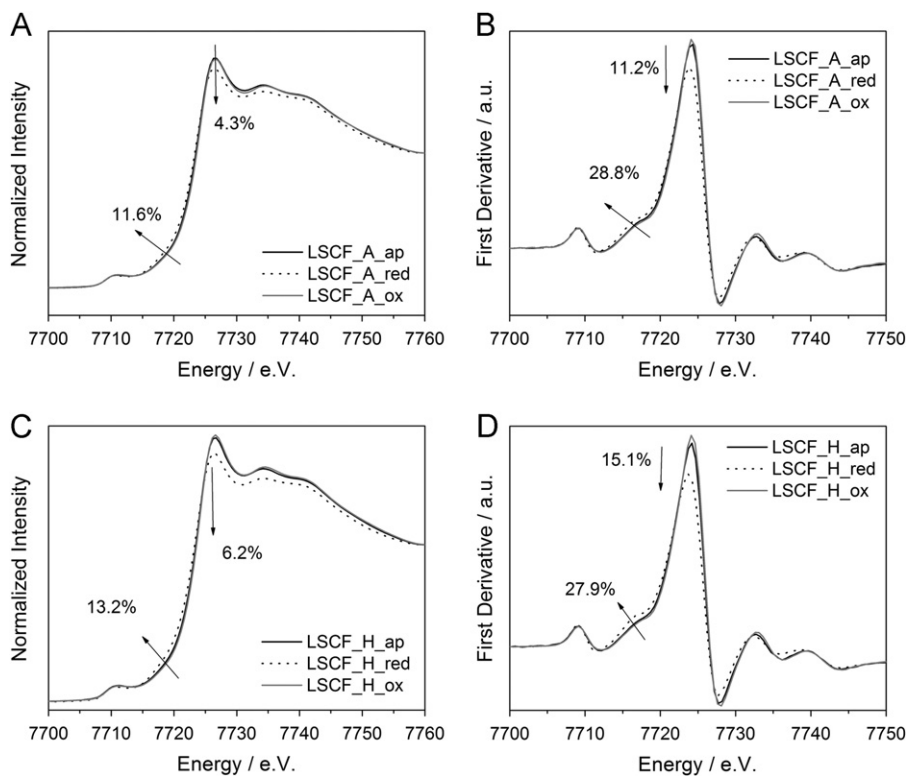


Fig. 3. Cobalt absorption coefficient (left) and first derivative (right) for the LSCF samples. The absorption intensity was normalized to 1 at 7760 eV for better comparison. (A) and (B) show samples synthesized by an acetate route and (C) and (D) show samples obtained with the novel HMTA method.

these two samples. *A priori*, it could be concluded that the synthesis method (acetate or HMTA) had no influence in the oxidation state and structural position of the Co atom in the final LSCF as prepared samples.

Regarding the different red–ox treatments applied to the LSCF samples (Fig. 3), the normalized WL intensity of the reduced samples resulted 4.3% and 6.2% smaller than in the oxidized samples for the acetate and the HTMA routes respectively (Fig. 3A and C). In addition, the intensity at the shoulder (feature II, in Fig. 2A) increases 11.6% and 13.2% respectively, and the change is even more evident when observing the first derivative intensities (Fig. 3B and D). Despite the small change, from the statistical considerations stated previously, the reduced LSCF samples (regardless of the synthesis method) can be considered significantly different from the not treated or the re-oxidized samples.

Toquin et al. [19] studied the oxidation of SrCoO_{2.5} to SrCoO₃ and reported an increase in the normalized intensity of the Co *K*-edge WL peak, which was interpreted as an increase in the coordination of the absorbing atom upon oxidation. In the cases studied here, the observed WL intensity decrease upon reduction in Ar can be interpreted in the same way as a reduction of the coordination around Co (i.e. a reduction of the atom formal oxidation state).

Indeed, a formal valence decrease associated with the transfer of intensity from the higher (IV) to the lower (II) energy features can be associated with modest changes in the *d*-orbital occupancy due to vacancy-induced high Co *d* count sites. An enhanced (II) intensity at expenses of (IV) would be presumably associated with the loss of *d*⁵/*d*⁶ character and gain of *d*⁷ character due to O-deficient sites in the Ar atmosphere [20]. Orikasa et al. recently reported a study on the compound La_{0.6}Sr_{0.4}CoO_{3-δ}, annealed at various oxygen partial pressures *p*(O₂) [2,3]. The authors observed a Co *K*-edge shift to lower energies with decreasing *p*(O₂) and proposed that this treatment introduced both oxygen vacancies creation and the reduction of the Co average valence. Our study in Fe doped cobaltites of the same perovskite family seems to be in good agreement with that observation, and are also in excellent accordance with the latest work of the same authors on La_{0.6}Sr_{0.4}Co_{0.8}Fe_{0.2}O_{3-δ} where the same tendency is observed analyzing the Co *K*- and *L*-edges [4]. Moreover, our results are also in accordance with the data recently presented by Itoh et al., who studied the *in-situ* reduction of the perovskite La_{0.6}Sr_{0.4}Co_{0.2}Fe_{0.8}O_{3-δ} between 1 atm ≤ *p*(O₂) ≤ 10⁻⁴ atm at 900 K and 1000 K [7,9]. Although those samples were synthesized at higher temperatures (i.e. have larger grain sizes than ours) the Co *K*-edge absorption spectra after reduction follow the same tendency as in our nano-sized LSCF samples, which were measured *ex-situ* after quenching from a reductive atmosphere. Indeed, these authors showed that the Co *K*-edge energy position measured at the half-high intensity shifts to lower energies upon reduction, and interpreted that also as a sign a reduction in the Co valence and increment in the oxygen deficiency.

On the other hand, the *as-prepared* and the *re-oxidized* spectra differ only 1% in intensity at the WL or the SH, and their edges are shifted maximum 0.2 eV. These values are in the order of the expected statistical dispersion due to measurements parameters and sample heterogeneity. Thus, the re-oxidized samples can be considered similar to the non-treated samples, in agreement with the reversibility observed according to XPD experiments.

More information about the 3*d* band occupancy may be obtained from the pre-edge peak intensity, full width at half maximum (FWHM) and centroid position. The 1*s* → 3*d* transition probability, reflected by the peak intensity, is related to the system symmetry and the occupancy of the 3*d* band [21]. Indeed, as shown in Fig. 2A metallic cobalt does not present any pre-edge peak, because there are no unoccupied 3*d* states for the transition (Co⁰: [Ar]3*d*⁷4*s*²), while CoO pre-edge peak (Co²⁺: [Ar]3*d*⁷,

octahedrally coordinated) is less intense than in the spinel Co₃O₄ (mixture of Co²⁺: [Ar]3*d*⁷ in tetrahedral sites and Co³⁺: [Ar]3*d*⁶ in octahedral sites) [22]. In this case, the baseline-subtracted pre-edge features (Fig. 2A, inset) can be well adjusted by convolution of Gaussian functions with around 2 eV FWHM: CoO and other reference materials containing Co²⁺ (not shown here) show a single pre-edge peak around 7709.0 eV, Co₃O₄ (composed of Co³⁺ and Co²⁺) presents additionally an extra component around 7711.4 eV, LaCoO₃ (Co³⁺) shows a wider pre-edge peak at 7710.6 eV, while BaCoO₃ (Co⁴⁺) presents a peak around 7709.8 eV. Although spectral form and edge position are not the same, LSCF pre-edge peaks are centered exactly in the same position as that of the LaCoO₃ (Co³⁺). The main difference is that the LSCF pre-edge peaks are more intense than that of the LaCoO₃ reference. The presence of two components in the pre-edge feature of LaCoO₃ was reported by many authors. The components were assigned alternatively to a Co 1*s* → 3*d* quadrupolar transition involving the splitting of *t*_{2*g*} and *e*_g levels [17,23] or to quadrupole-allowed Co 1*s* → *e*_g[↑] and *e*_g[↓] transitions involving spin changes [18]. In our case, it is not possible to resolve the presence of two components, neither in LaCoO₃ nor in LSCF samples. However, convolution of Gaussian peaks with FWHM between 1.5 and 2.5 eV resulted in two components centered around 7710 and 7712 eV, in accordance with the data mentioned above. These components can be also found in all LSCF samples and support a closer similarity between the 3*d* band of the LSCF nano-grains and LaCoO₃. Regarding the intensity differences, Moen et al. [21] showed that for a given occupancy, the 1*s* → 3*d* transition probability increases when the coordination environment of the absorbing atom lacks of inversion symmetry. Thus, the slightly intensity enhancement observed in the pre-edge peaks of LSCF samples may reflect a loss of symmetry respect to Co in a regular octahedral environment.

3.2.2. Iron XANES

The general Fe *K*-edge absorption coefficient of LSCF samples (Fig. 2B) is very similar to that observed for the element Co (Fig. 2A). The main absorption (WL) occurs at 7130.2 eV due transitions from 1*s* to 4*p* states. A slope change at lower energies (shoulder of the first derivative) occurs around 7121.1 eV and was associated to 1*s* to 4*p*-like states transitions above the Fermi level [24]. A pre-peak feature appears at 7114.9 eV. This absorption is usually attributed to quadrupole transitions from the 1*s* core level to the 3*d* empty states of the iron, with contribution of dipole transitions due to hybridized states provided by oxygen neighboring atoms in octahedral coordination [25].

Compared to other Fe-bearing compounds with oxidation states between Fe⁰ and Fe³⁺ the *K*-edge position and the pre-edge centroid (inset in Fig. 2B) of both LSCF samples appear at higher energies, supporting higher oxidation states of the absorbent atom.

It was previously demonstrated that Fe *K*-pre-edge characteristics (such as position, shape or number of components) can be related to the iron oxidation state and its coordination [26]. Pre-edge (Fig. 2B, inset) of Fe²⁺ bearing reference materials show a feature around 7112.5 eV, while it appears at higher energies (approximately 7114.5 eV) in those materials containing Fe³⁺. LSCF samples present a wide pre-edge peak which can be decomposed in two Gaussian functions (FWHM=2 eV) centered in 7114.4 eV and 7116.1 eV respectively. The first one may be associated to the presence of Fe³⁺ while the second one is probably related to higher oxidation states of the metal. Indeed, Berry et al. [27] reported a mixture of Fe³⁺/Fe⁴⁺ in the La_{0.5}Sr_{0.5}-FeO₃ perovskite and Blasco et al. [28] showed that the oxidation state of Fe in the family La_{1-x}Sr_xFeO_{3-δ} (0 < *x* < 1) can be

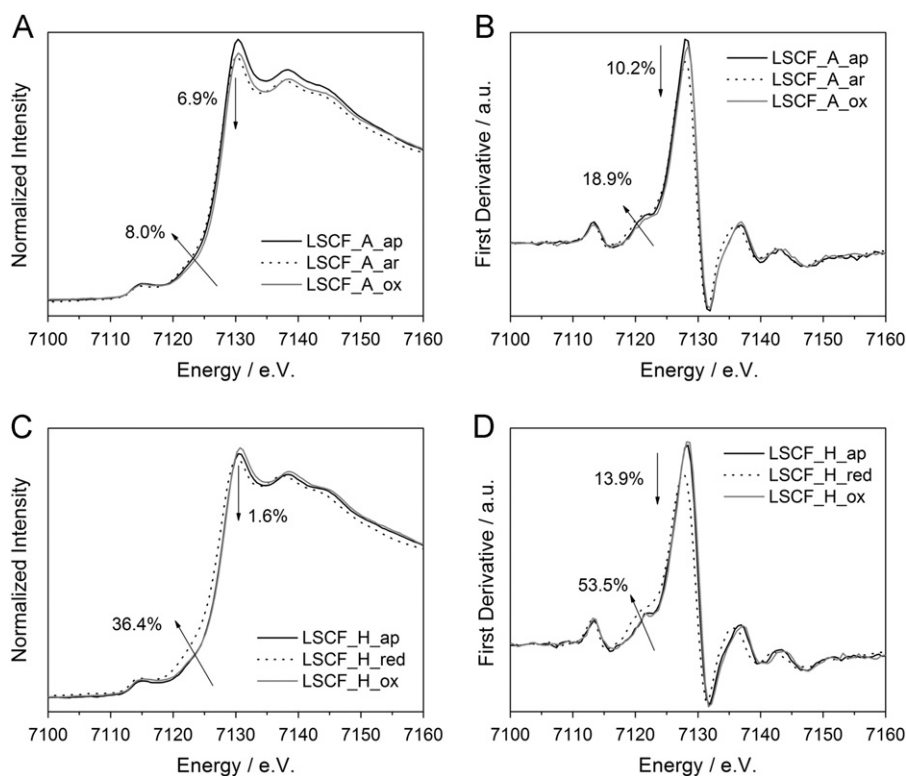


Fig. 4. Iron absorption coefficient (left) and first derivative (right) for the LSCF samples. The absorption intensity was normalized to 1 at 7160 eV for better comparison. (A) and (B) show samples synthesized by an acetate route and (C) and (D) show samples obtained with the novel HMTA method.

described either by a bimodal distribution of formal Fe^{3+} and Fe^{4+} ions or by an $\text{Fe}^{3.x+}$ intermediate valence.

Regarding the thermal treatments under reductive and oxidative atmospheres (Fig. 4), the general behavior follows the tendency observed for cobalt: an intensity transfer from the white line to lower energies appears upon reduction, indicating a decrease of the Fe formal oxidation state or changes in the coordination environment around the Fe atoms [4,7,8]. Compared to the intensity of the untreated samples, the WL (SH) intensity decreases (increases) 6.9% (8.0%) in the *LSCF_A* samples and 1.6% (36.4%) in the *LSCF_H* samples under reducing atmospheres. In addition, the WL position does not change appreciably, but the SH moves 0.3 eV and 1.5 eV towards lower energies, respectively. This tendency, however, seems to be more pronounced in the HMTA rather than in the acetate samples. This fact is even more evident looking to the changes in the first derivative intensities and positions of reduced samples against the untreated ones (Fig. 4B and D): there is a decrease of 10.2% (*LSCF_A*) and 13.9% (*LSCF_H*) of the first maximum intensity and an increase of 18.9% (*LSCF_A*) and 53.2% (*LSCF_H*) of the shoulder intensity. Differently from the Co results, the process for Fe was not totally reversible for the acetate samples: the *LSCF_A_ox* sample does not result exactly like the *LSCF_A_ap* one. However, it is worth to note that the results from iron have larger uncertainties than the ones from cobalt, because it is four times less concentrated.

In addition to these general features, it is worth to note that the pre-edge peak centroid at 7114.9 eV in the *as prepared* or *re-oxidized* LSCF samples moves upon the reducing treatment to 7114.4 eV and 7114.2 eV in the acetate and the HMTA samples respectively (data not shown). A similar behavior was observed also for $\text{La}_{0.5}\text{Sr}_{0.5}\text{FeO}_3$ perovskites after treatment in a reducing H_2 atmosphere and was explained by a reduction of Fe^{4+} to Fe^{3+} in that compound [27].

3.2.3. Cobalt and iron oxidation state in the perovskites B-site

Analysis of the spectral features and edge position can be used to find the electronic structure of the absorbing atom and its coordination environment in LSCF. The *K*-edge positions are particularly sensible to the oxidation states of the transition metals. Generally, the edge shifts to higher energies for higher oxidation states, in agreement with a strong d-hole creation. In the case of cobalt for example, Co oxides, nitrates, fluorides, carbonates, etc. are often used to calibrate the Co valence with the absorption edge energy [29,30]. However, it is well known that the applicability of a XANES calibration for determining an oxidation state depends strongly on the coordination environment of the target atom [31]. Indeed, if only metallic Co, Co oxides (CoO and Co_3O_4) and Co perovskites structures (LaCoO_3 and BaCoO_3) are taken into account, the position of the first maximum of the first derivative spectrum shows an approximately linear relation with the formal valence of the Co atom (Fig. 5A, dotted line). An equivalent behavior is found for iron (Fig. 5B, dotted line).

In order to get a better calibration for the LSCF samples, we decided to use only references with Co and Fe in a perovskites structure for the calibration. For that, carefully selected published² data were also included in the calculation.

Cobalt reference materials from literature corresponding to the LSCF family (or with the metal cation occupying a crystalline environment with stronger resemblance to that of the perovskite studied here) show edge positions between 7723 and 7726 eV for oxidation states between Co^{3+} and Co^{4+} (Fig. 5A, open symbols). These edges are in excellent agreement with the LaCoO_3 and

² We only included references where the oxidation state of the cation was determined by an independent method and the edge position could be referenced to the metallic compound.

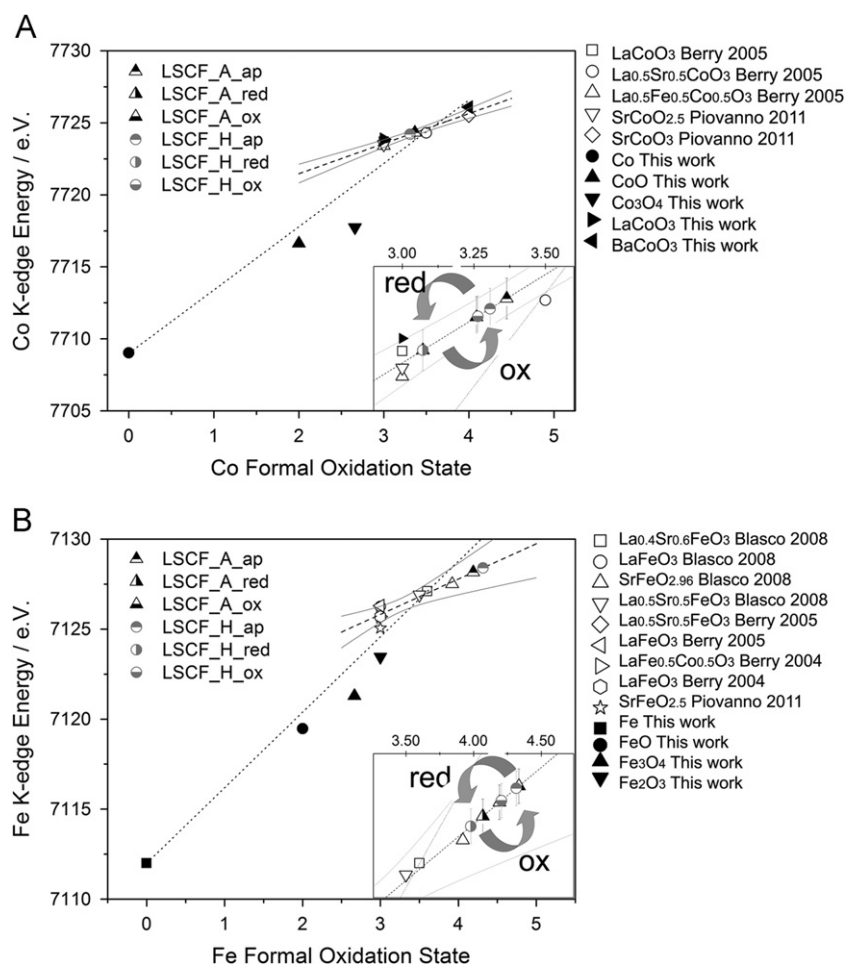


Fig. 5. Cobalt (A) and iron (B) absorption edge energy vs. formal oxidation states, including measured reference samples (closed symbols) and literature data (open symbols) [27,28,34,35]. The edge position was considered as the position of the first maximum of the first derivative spectra. The dotted lines show the linear fit including all references. The dashed lines show a linear fit including only references with valence states between 3+ and 4+, the gray lines are the 95% confidence band of the latter calibration curves. The insets in (A) and (B) show an enlarged view of the region of interest.

BaCoO₃ spectra measured here (Fig. 5A, close symbols). Using the linear calibration obtained in this way (Fig. 5A, dashed line), the Co oxidation state in the *as-prepared* samples result Co^{3.36+} and Co^{3.31+} for the LSCF samples synthesized by the Acetate and by the HMTA routes, respectively. The reduced materials present slight lower values (Co^{3.07+}), and the formal valence returns back near the original position (Co^{3.26+}) upon re-oxidation in both cases. This observation is in excellent agreement with the general behavior mentioned above and supports (i) that a reduction process, although very small, is present and (ii) that the red-ox cycle are reversible.

Fig. 5B shows the calibration curve for iron, in which reference data from the literature were also included for better accuracy at higher oxidation states. In average, iron in LSCF *as prepared* material is found as Fe^{4.25+} and the formal valence decreases to Fe^{4.02+} upon reduction. In the *re-oxidized* samples the formal oxidation state moves again to values closer to the original *as prepared* material. This formal oxidation state is much higher than the (3.6+) expected at the B-site from the stoichiometric relation in La_{0.4}Sr_{0.6}(Co,Fe)O₃. Although the formation of Fe⁴⁺ and larger average valence of Fe than Co were reported for La_{0.6}Sr_{0.4}Co_{0.8}Fe_{0.2}O_{3-δ} [4], we did not discard the presence of a systematic error in the calculation of the Fe valences, due to the lack of measured reference materials with perovskite structure and higher Fe oxidation states for the calibration.

Fig. 6A resumes the results obtained for iron and cobalt oxidation states in LSCF samples, for the two synthesis methods

tested here. The *reduced* samples show in all cases lower valences than the *as-prepared* powders and the *re-oxidized* samples present oxidation states near the initial values. Notably, XANES allow detecting that Co and Fe are not equivalent for the perovskite B-site. Although both elements react decreasing their valences upon reduction, the former is always in an oxidation state much closer to 3+ than to 4+, as is the case of the latter one. This behavior is in excellent agreement with recent studies of the Co/Fe valences in LSCF systems [4,7,9]. The mean B-site valence of the ABO₃ perovskites can be calculated as 0.8 times the cobalt valence plus 0.2 times the iron valence. This calculation shows that, although both metals have different valences, they combine in a way such that the nano-sized LSCFs composition is closer to La_{0.4}Sr_{0.6}(Co_{0.8}Fe_{0.2})^{3.52+}O_{2.96} for the *as prepared* materials, without larger differences between both syntheses methods tested here. This formal oxidation state is relatively close to the (3.6+) expected at the B-site from the stoichiometric relation in La_{0.4}Sr_{0.6}(Co,Fe)O₃. The fact that the absolute Fe valences may be overestimated by a systematic error in the calibration is minimized in the B-site oxidation state value calculation because Fe is four times less concentrated than Co in these materials.

In addition, it could be shown that the average composition changes to La_{0.4}Sr_{0.6}(Co_{0.8}Fe_{0.2})^{3.26+}O_{2.83} when a *reducing* treatment is applied; it seems that the LSCF material responds to the reducing environment with the creation of oxygen vacancies and both transition metal's oxidation states moves toward lower

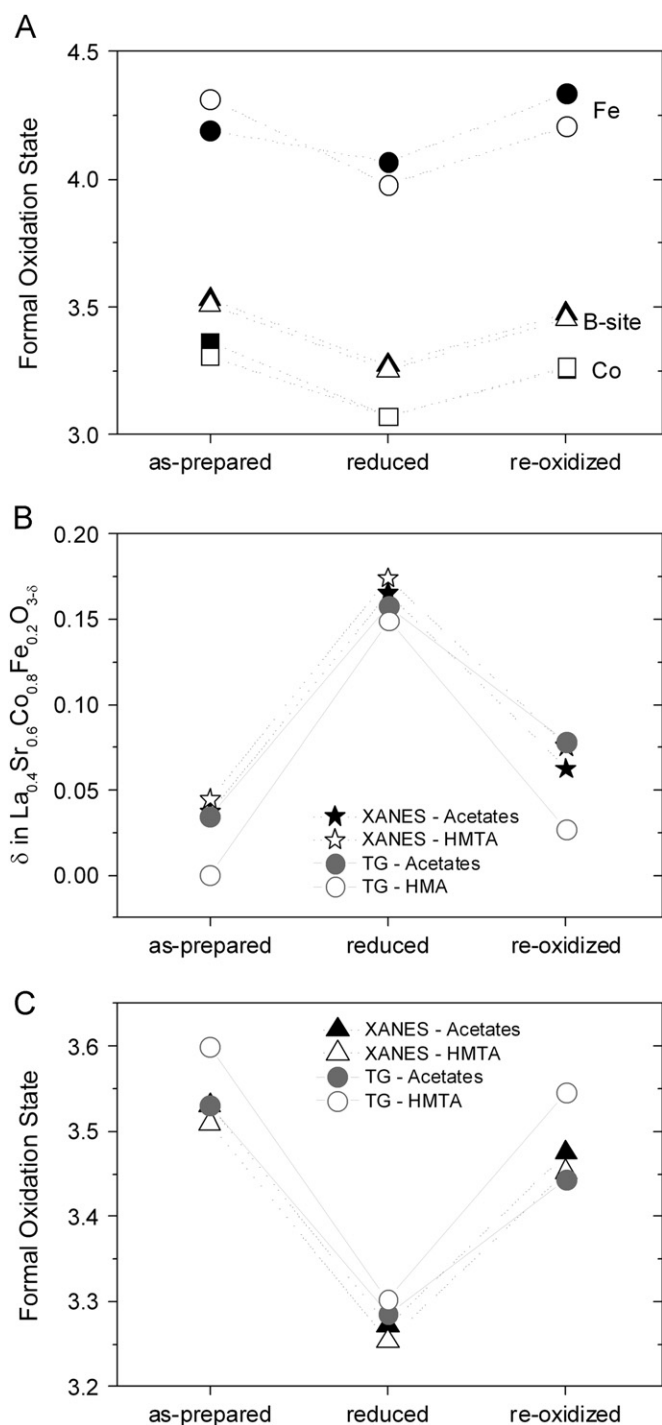


Fig. 6. (A) XANES-measured formal oxidation state for cobalt and iron in LSCF samples synthesized by the acetate (close symbols) and the HMTA (open symbols) routes. The triangles show the calculated B-site average valence of the ABO_3 perovskites. (B) Oxygen deficiency in LSCF_A and LSCF_H samples; the circles show the oxygen deficiency calculated using thermogravimetric balance (TG) measurements; the stars show the results obtained using the XANES data. (C) Comparison of the B-site average valence using the XANES and the TG data. Values shown in these figures can be found also as a table in the supplementary on-line material.

values, compensating for charge changes. This property seems to be distinctive from the nano-sized LSCF. LSCF powders synthesized at higher temperatures (i.e. bigger grain sizes) show a preferential reduction of Co over Fe upon reduction [4,7,9] that was not clearly detected here. The red-ox process in nano-sized

LSCF is reversible, because the composition returns closer to the as prepared material after the re-oxidation treatment.

Oxygen stoichiometry from two selected samples (*LSCF_H_red* and *LSCF_H_ox*) samples was checked by an independent method: thermogravimetric (TG) analysis (Fig. 6B) as described in the experimental section. Sample compositions resulted $La_{0.4}Sr_{0.6}Co_{0.8}Fe_{0.2}O_{2.85}$ ($\delta=0.15$) and $La_{0.4}Sr_{0.6}Co_{0.8}Fe_{0.2}O_{2.97}$ ($\delta=0.03$) for *LSCF_H_red* and *LSCF_H_ox*, and $La_{0.4}Sr_{0.6}Co_{0.8}Fe_{0.2}O_{2.84}$ ($\delta=0.16$) and $La_{0.4}Sr_{0.6}Co_{0.8}Fe_{0.2}O_{2.92}$ ($\delta=0.08$) for *LSCF_A_red* and *LSCF_A_ox*, respectively. These δ values (circles in Fig. 6B), are in excellent accordance with the reported data for $La_{0.6}Sr_{0.4}Co_{0.8}Fe_{0.2}O_{3-\delta}$ at 10^5 Pa and 10 Pa [4]. Although the values from the thermogravimetric analysis follows the trend of the XANES data (stars in Fig. 6B), they are systematically smaller. We attribute the difference to calibration uncertainties in both methods (which is indeed in the order of 15–20%). However, despite this difference in the absolute values, the comparison of the relative δ values at the reduced and the re-oxidized states ($\Delta\delta_{XANES}=0.099$, $\Delta\delta_{TG}=0.122$ for HMTA and $\Delta\delta_{XANES}=0.10$, $\Delta\delta_{TG}=0.08$ for acetate) differ in less than 20%. Moreover, Fig. 6C shows that the XANES calculated B-site average valence (triangles) is, inside the related uncertainties, identical to the one calculated from the hydrogen reduction in the thermobalance (circles), supporting the methodology applied here.

4. Conclusion

Synchrotron X-ray absorption techniques such as XANES are increasingly recognized by the Fuel Cell community as powerful tools to examine the oxidation state and coordination chemistry of the metals involved in the transport of electrons and ions in the electrode materials. This information is thus helpful for reconstructing the electronic configuration and sample stoichiometry, determining in this way the influence on certain synthesis and function parameters variation in the fuel cell performance. Moreover, this technique is interesting because allows distinguishing whether or not doping elements repeat the main component's behavior.

In this case we analyzed the nano-sized mixed conductor $La_{0.4}Sr_{0.6}Co_{0.8}Fe_{0.2}O_{3-\delta}$. We demonstrated using a combination of XANES and XPD results that this material reacts differently under reductive or oxidative atmospheres. A treatment under Ar at 500 °C for 24 h produced structural changes in the material, resulting in the co-existence of the rhombohedral $R\bar{3}c$ with another oxygen vacancy ordered phase. Using XANES at the Co and Fe *K*-edge we have determined that this transformation implies modification of the near environment of the Co/Fe atoms. Intensity shifts in the Co and Fe *K*-edge features under reductive atmosphere might be explained by a change in the formal valence of the transition metal atoms to lower oxidation states, together with the formation of oxygen vacancies. In addition, we observed the reversibility of this transformation: the spectral features of re-oxidized samples did not differ significantly from the untreated samples. This behavior was observed in the material synthesized by an acetate as well as by the novel HTMA routes and can be attributed to intrinsic micro structural defects (size and strain) related to the nanometric size of the material.

Acknowledgments

The authors thank D. Lamas, L. Acuña and J. Geck for their helpful assistance in the experimental design, the analysis of the data and the improvement of this manuscript. XAS measurements were financed by the LNLS proposal D04B-XAFS1-9932 (2010).

Appendix A. Supporting information

Supplementary data associated with this article can be found in the online version at <http://dx.doi.org/10.1016/j.jssc.2012.10.019>.

References

- [1] L.W. Tai, M.M. Nasrallah, H.U. Anderson, D.M. Sparlin, S.R. Sehlín, *Solid State Ion.* 76 (1995) 273–283.
- [2] Y. Orikasa, T. Ina, T. Nakao, A. Mineshige, K. Ameszawa, M. Oishi, H. Arai, Z. Ogumi, Y. Uchimoto, *ECS Trans.* 13 (2008) 201–205.
- [3] Y. Orikasa, T. Ina, T. Nakao, A. Mineshige, K. Ameszawa, M. Oishi, H. Arai, Z. Ogumi, Y. Uchimoto, *J. Phys. Chem. C* 115 (2011) 16433–16438.
- [4] Y. Orikasa, T. Ina, T. Nakao, A. Mineshige, K. Ameszawa, M. Oishi, H. Arai, Z. Ogumi, Y. Uchimoto, *Phys. Chem. Chem. Phys.* 13 (2011) 16637–16643.
- [5] L. Baqué, A. Caneiro, M.S. Moreno, A. Serquis, *Electrochem. Commun.* 10 (2008) 1905–1908.
- [6] N. Grunbaum, L. Dessemond, J. Fouletier, F. Prado, A. Caneiro, *Solid State Ion.* 177 (2006) 907–913.
- [7] T. Itoh, M. Nakayama, *J. Solid State Chem.* 192 (2012) 38–46.
- [8] T. Itoh, S. Shirasaki, H. Ofuchi, S. Hirayama, T. Honma, M. Mori, M. Nakayama, *J. Fuel Cell Sci. Technol.* 9 (2012) 031004.
- [9] T. Itoh, S. Shirasaki, H. Ofuchi, S. Hirayama, T. Honma, M. Nakayama, *Solid State Commun.* 152 (2012) 278–283.
- [10] A. Mineshige, J. Abe, M. Kobune, Y. Uchimoto, T. Yazawa, *Solid State Ion.* 177 (2006) 1803–1806.
- [11] J.P. Hoges, *J. Solid State Chem.* 151 (2000) 190–209.
- [12] F. Prado, N. Grunbaum, A. Caneiro, A. Manthiram, *Solid State Ion.* 167 (2004) 147–154.
- [13] H.E. Shinawi, J.F. Marco, F.J. Berry, C. Greaves, *J. Mater. Chem.* 20 (2010) 3253–3259.
- [14] L. Baqué, F. Napolitano, A. Soldati, D. Lamas, A. Caneiro, A. Serquis, *Activity Report 2010: LNLS/Brazilian Synchrotron Light Laboratory*. Available from: <<http://www.lnls.br/ar2010>>, 2010, p. 1663.
- [15] J. Rodríguez-Carvajal, *Physica B* 192 (1993) 55.
- [16] F. de Groot, *Chem. Rev.* 101 (2001) 1779–1808.
- [17] M. Medarde, C. Dallera, M. Grioni, J. Voigt, A. Podlesnyak, E. Pomjakushina, K. Conder, T. Neisius, O. Tjernberg, S.N. Barilo, *Phys. Rev. B* 73 (2006) 054424.
- [18] S.K. Pandey, A. Kumar, S. Khalid, A.V. Pimpale, *J. Phys: Condens. Mater.* 18 (2006) 7103–7113.
- [19] R.L. Toquin, W. Paulus, A. Cousson, C. Prestipino, C. Lamberti, *J. Am. Chem. Soc.* 128 (2006) 13161–13174.
- [20] J.E. Sunstrom, K.V. Ramanujachary, M. Greenblatt, M. Croft, *J. Solid State Chem.* 139 (1998) 388–397.
- [21] A. Moen, D.G. Nicholson, B.S. Clausen, P.L. Hansen, A. Molenbroek, G. Steffensen, *Chem. Mater.* 9 (1997) 1241–1247.
- [22] R.G. Burns, *Mineralogical Applications of Crystal Field Theory*, University Press, Cambridge, 1970.
- [23] G. Thornton, B.C. Toffield, A.W. Hewat, *J. Solid State Chem.* 61 (1986) 301–307.
- [24] H. Purdum, P.A. Montano, G.K. Shenoy, T. Morrison, *Phys. Rev. B* 25 (1982) 4412–4417.
- [25] Z.Y. Wu, D.C. Xian, T.D. Hu, Y.N. Xie, Y. Tao, C.R. Natoli, E. Paris, A. Marcelli, *Phys. Rev. B* 70 (2004) 033104.
- [26] P.-E. Petit, F. Farges, M. Wilke, V.A. Solé, *J. Synch. Radiat.* 8 (2001) 952–954.
- [27] F.J. Berry, J.F. Marco, X. Ren, *J. Solid State Chem.* 178 (2005) 961–969.
- [28] J. Blasco, B. Aznar, J. García, G. Subías, J. Herrero-Martín, J. Stankiewicz, *Phys. Rev. B* 77 (2008) 054107.
- [29] V. Vashook, D. Franke, J. Zosel, L. Vasylechko, M. Schmidt, U. Guth, *J. Alloys Compd.* 487 (2009) 577–584.
- [30] J.M. Ramallo-López, E.J. Lede, F.G. Requejo, J.A. Rodríguez, J.-Y. Kim, R. Rosas-Salas, J.M. Domínguez, *J. Phys. Chem. B* 108 (2005) 20005–20010.
- [31] A. Berry, H.S.C. O’Neil, K.D. Jayasuriya, S.J. Campbell, G.J. Foran, *Am. Min.* 88 (2003) 967–977.
- [32] A. Caneiro, P. Bavadz, J. Fouletier, J.P. Abriata, *Rev. Sci. Instrum.* 53 (1982) 1072.
- [33] A. Caneiro, *J. Appl. Electrochem.* 11 (1981) 83.
- [34] F.J. Berry, J.R. Gancedo, J.F. Marco, X. Ren, *J. Solid State Chem.* 177 (2004) 2101–2114.
- [35] A. Piovano, G. Agostini, A.I. Frenkel, T. Bertier, C. Prestipino, M. Ceretti, W. Paulus, C. Lamberti, *J. Phys. Chem.* 115 (2011) 1311–1322.